








Cellular contribution to left and right atrial dysfunction in chronic arterial hypertension in pigs

Ge Jin^{1,2} , Martin Manninger¹ , Gabriel Adelsmayr³ , Michael Schwarzl¹, Alessio Alogna^{4,5}, Patrick Schönleitner¹, David Zweiker¹, Florian Blaschke^{4,5}, Mohammad Sherif⁴, Snjezana Radulovic¹, Paulina Wakula^{4,5} , Sylvia Schauer⁶, Gerald Höfler⁶, Ursula Reiter³, Gert Reiter⁷, Heiner Post^{4,5}, Daniel Scherr¹ , Karoly Acsai⁸, Gudrun Antoons⁹, Burkert Pieske^{4,5,10}  and Frank R. Heinzel^{4,5*} 

¹Division of Cardiology, Medical University of Graz, Graz, Austria; ²The Second Affiliated Hospital and Yuying Children's Hospital of Wenzhou Medical University, Wenzhou, China; ³Department of Radiology, Medical University of Graz, Graz, Austria; ⁴Department of Internal Medicine and Cardiology, Charité—Universitätsmedizin Berlin, Campus Virchow-Klinikum, Augustenburgerplatz 1, Berlin, 13353, Germany; ⁵DZHK (German Centre for Cardiovascular Research), partner site Berlin, Berlin, Germany; ⁶Department of Pathology, Medical University of Graz, Graz, Austria; ⁷Research & Development, Siemens AG Healthcare, Vienna, Austria; ⁸Division of Pharmacology and Pharmacotherapy, University of Szeged, Szeged, Hungary; ⁹Faculty of Sciences, Department of Organic and Macromolecular Chemistry, Ghent University, Ghent, Belgium; and ¹⁰Department of Cardiology, German Heart Center Berlin (DHZB), Berlin, Germany

Abstract

Aims Atrial contractile dysfunction contributes to worse prognosis in hypertensive heart disease (HHD), but the role of cardiomyocyte dysfunction in atrial remodelling in HHD is not well understood. We investigated and compared cellular mechanisms of left (LA) and right atrial (RA) contractile dysfunction in pigs with HHD.

Methods and results *In vivo* electrophysiological and magnetic resonance imaging studies were performed in control and pigs treated with 11-deoxycorticosterone acetate (DOCA)/high-salt/glucose diet (12 weeks) to induce HHD. HHD leads to significant atrial remodelling and loss of contractile function in LA and a similar trend in RA (magnetic resonance imaging). Atrial remodelling was associated with a higher inducibility of atrial fibrillation but unrelated to changes in atrial refractory period or fibrosis (histology). Reduced atrial function in DOCA pigs was related to reduced contraction amplitude of isolated LA (already at baseline) and RA myocytes (at higher frequencies) due to reduced intracellular Ca release (Fura 2-AM, field stimulation). However, Ca regulation differed in LA and RA cardiomyocytes: LA cardiomyocytes showed reduced sarcoplasmic reticulum (SR) [Ca], whereas in RA, SR [Ca] was unchanged and SR Ca²⁺-ATPase activity was increased. Sodium–calcium exchanger (NCX) activity was not significantly altered. We used ORM-10103 (3 μM), a specific NCX inhibitor to improve Ca availability in LA and RA cardiomyocytes from DOCA pigs. Partial inhibition of NCX increased Ca²⁺ transient amplitude and SR Ca in LA, but not RA cells.

Conclusions In this large animal model of HHD, atrial remodelling in sinus rhythm *in vivo* was related to differential LA and RA cardiomyocyte dysfunction and Ca signalling. Selective acute inhibition of NCX improved Ca release in diseased LA cardiomyocytes, suggesting a potential therapeutic approach to improve atrial inotropy in HHD.

Keywords Atrial remodelling; Calcium; Cardiomyocytes; Contractility; Sodium–calcium exchanger

Received: 12 February 2020; Revised: 2 September 2020; Accepted: 22 October 2020

*Correspondence to: Frank R. Heinzel, Department of Internal Medicine and Cardiology, Charité—Universitätsmedizin Berlin, Campus Virchow-Klinikum, Augustenburgerplatz 1, 13353 Berlin, Germany. Email: frank.heinzel@charite.de

Introduction

The heart's atria contribute to ventricular filling and cardiac output, determine heart rhythm, and participate in endocrine signalling. Atrial remodelling has been largely investigated as a substrate for atrial fibrillation (AF). However, the pivotal

role of atrial dysfunction in the development of heart failure (HF) even in the absence of AF is increasingly recognized.¹ Indeed, atrial contractile dysfunction in HF is associated with reduced exercise capacitance and worse prognosis.^{2–4}

Important clinical triggers of atrial remodelling are increased mechanical load and neurohumoral activation, as

seen in HF and also in early cardiac remodelling as a result of systemic arterial hypertension and increased left ventricular (LV) pressure. Indeed, left atrial (LA) enlargement is present in about one-third of hypertensive patients,⁵ and interestingly, the right atrium (RA) is also involved.⁶

The pathophysiology of atrial remodelling is complex and likely aetiology specific but has been mainly studied in animal models of AF or chronic HF.⁷ AF is a clinically relevant manifestation of atrial remodelling,¹ and also contributes to its progression. AF reduces the atrial effective refractory period (AERP), thus promoting AF sustainability ('AF begets AF'⁸). The effects of other clinical conditions such as arterial hypertension and ageing on atrial remodelling are less well understood. We have shown that in the presence of AF, the induction of arterial hypertension worsens atrial remodelling and arrhythmogeneity, however, without further shortening of AERP.⁹ Arterial hypertension also promotes atrial remodelling independent of AERP in aged rats.¹⁰

While systemic arterial hypertension is sufficient to initiate maladaptive LA and RA remodelling,^{5,6,11} cellular mechanisms have not yet been investigated in a large animal model. Studies in rat suggest impairment of LA cardiomyocyte Ca^{2+} homeostasis.^{12,13} Pigs have a cardiac anatomy more close to humans. In the present study, we therefore characterized the functional and cellular adaptation of the LA and RA to moderate systemic arterial hypertension in pigs to test the hypothesis that atrial dysfunction *in vivo* is associated with contractile dysfunction of atrial cardiomyocytes. In addition, we explore an approach to improve cardiomyocyte Ca^{2+} signalling in hypertensive atrial remodelling using a novel inhibitor of sarcolemmal Na^+/Ca^{2+} exchanger (NCX).

Methods

Animal handling was in accordance with the Guide for the Care and Use of Laboratory Animals (National Institutes of Health, USA). Experimental protocols were approved by the local bioethics committee of Vienna, Austria (BMWF-66.010/0108-II/3b/2010, BMWF-66.010/0128-II/3b/2012, and BMWF-66.010/0091-II/3b/2013).

Experimental model

To induce arterial hypertension and hypertensive heart disease (HHD), 16 female landrace pigs (10–14 weeks of age) were treated with 11-deoxycorticosterone acetate (DOCA), combined with a high-sugar/salt/potassium diet (300 g sugar, 40 g salt, and 6 g potassium per day) for 12 weeks. DOCA pellets with a 90 day release (Innovative Research of America, USA) were implanted subcutaneously in the inguinal region under sedoanalgesia with ketamine (20 mg/kg body weight) and midazolam (0.25 mg/kg). Healthy pigs ($n = 31$)

of comparable weight were used as control (CTRL, 70 ± 6 vs. 60 ± 9 kg at the time of the final experiment). Supporting Information, *Figure S1* summarizes the use of animals for the experimental protocols.

Final experiment

A group of seven DOCA and eight CTRL pigs were sedated with ketamine and midazolam as stated earlier. Non-invasive blood pressure measurements were performed by tail cuff sphygmomanometry. Endotracheal intubation was performed after intravenous administration of propofol 1% (0.1 mL/kg). Narcosis was sustained with sevoflurane (1.5–2.5%), fentanyl (35 μ g/kg/h), midazolam (1.2 mg/kg/h), ketamine (2–8 mg/kg/h), and pancuronium (0.2 mg/kg/h). A balanced crystalloid infusion was administered at a fixed rate of 10 mL/kg/h. After instrumentation, a bolus of heparine (100 IE/kg) was administered, followed by a continuous infusion of 100 IE/kg/h.

In vivo electrophysiological studies

Pigs were then instrumented with a quadripolar stimulation catheter (5F Boston Scientific) in the high RA and a decapolar catheter (6F Decapolar, Biosense Webster) in the coronary sinus. AERP was determined by an S1–S2 stimulation protocol (1 ms pulse at twice diastolic threshold at cycle lengths 400, 300, and 240 ms). Inducibility of AF was assessed by burst protocols (1 ms pulse at four times diastolic threshold, cycle lengths 200/150/100/50 ms, 10 s duration, and five repetitions). An AF episode was defined as the onset of irregular atrial electrograms with an average cycle length shorter than 150 ms for more than 10 s.

Magnetic resonance imaging studies

After EP studies, six DOCA and a subgroup of seven CTRL pigs underwent magnetic resonance imaging using a 3T MR system (Magnetom Trio, Siemens Healthcare, Erlangen, Germany). Cardiac function was assessed from retrospectively electrocardiogram-gated, two-dimensional segmented FLASH (fast low-angle shot) cine images obtained under free breathing, using two-fold averaging to suppress breathing artefacts. For LV function and muscle mass assessment, the LV was covered by gapless slices in short-axis orientation (measured temporal resolution 27 ms interpolated to 40 cardiac phases per cardiac cycle; echo time, 2.7 ms; flip angle, 20°; and voxel size, $1.9 \times 1.6 \times 8.0$ mm³), and for atrial function evaluation, LA and RA were covered by gapless slices in long-axis orientation (measured temporal resolution 45 ms interpolated to 25 cardiac phases per cardiac cycle; echo time, 2.9 ms; flip angle, 15°; and voxel size, $2.5 \times 1.8 \times 4.0$ mm³).

Left ventricular function parameters [end-diastolic volume, LV end-diastolic volume; end-systolic volume, LV end-systolic volume; ejection fraction (EF), and LVEF], LV mass (including papillary muscles and trabecles to the myocardium), and atrial volumes were derived by manual segmentation (Figure 1A) using the Simpson approach (Argus, Siemens, Erlangen, Germany). LA and RA maximum, minimum, and before contraction (V_{bc}) volumes were derived from respective volume vs. time curves (Figure 2B). Pulmonary veins and mitral valve area were excluded from left, vena cava inferior/superior, coronary sinus, and tricuspid valve area from RA volumes by straight cut planes. Total EF is defined as total filling volume divided by the maximum volume, the passive EF as passive emptying volume divided by the maximum volume, and the contractile EF as active

emptying volume divided by the volume before contraction (in per cent).

Cell isolation

All chemicals were obtained from Sigma-Aldrich, Germany, if not stated otherwise. For organ explantation, pigs were premedicated as described earlier. Endotracheal intubation was performed after intravenous administration of propofol 1% (0.1 mL/kg). Narcosis was sustained with fentanyl (35 μ g/kg/h) and midazolam (1.2 mg/kg/h), and boli of heparine (100 IE/kg) and pancuronium (0.2 mg/kg) were administered. The heart was removed via thoracotomy and kept in cardioplegic solution (in mM: NaCl 130, KCl 27, MgSO₄

Figure 1 Left (LA) and right atrial (RA) remodelling and function in chronic arterial hypertension. (A) Long-axis magnetic resonance imaging images at the centre of the mitral valve (MV, left) and tricuspid valve (TV, right). Segmentation of left (solid line) and right (dashed line) atrial areas for volumetric assessment. (B) Schematic drawing of the atrial volume vs. time curve. Maximum volume, minimum volume, and volume before contraction (V_{bc}) are indicated (see Methods). Left and right maximal (C), minimal (D) volumes, and volumes before contraction (E) as well as total (F), passive (G), and contractile (H) ejection fraction (EF) from magnetic resonance imaging analysis of seven control (CTRL) and six 11-deoxycorticosterone acetate (DOCA) pigs (mean \pm standard error of the mean, * $P < 0.05$). CS, cell shortening; LV, left ventricular; PV, pulmonary vein; RV, right ventricular; VC, vena cava.

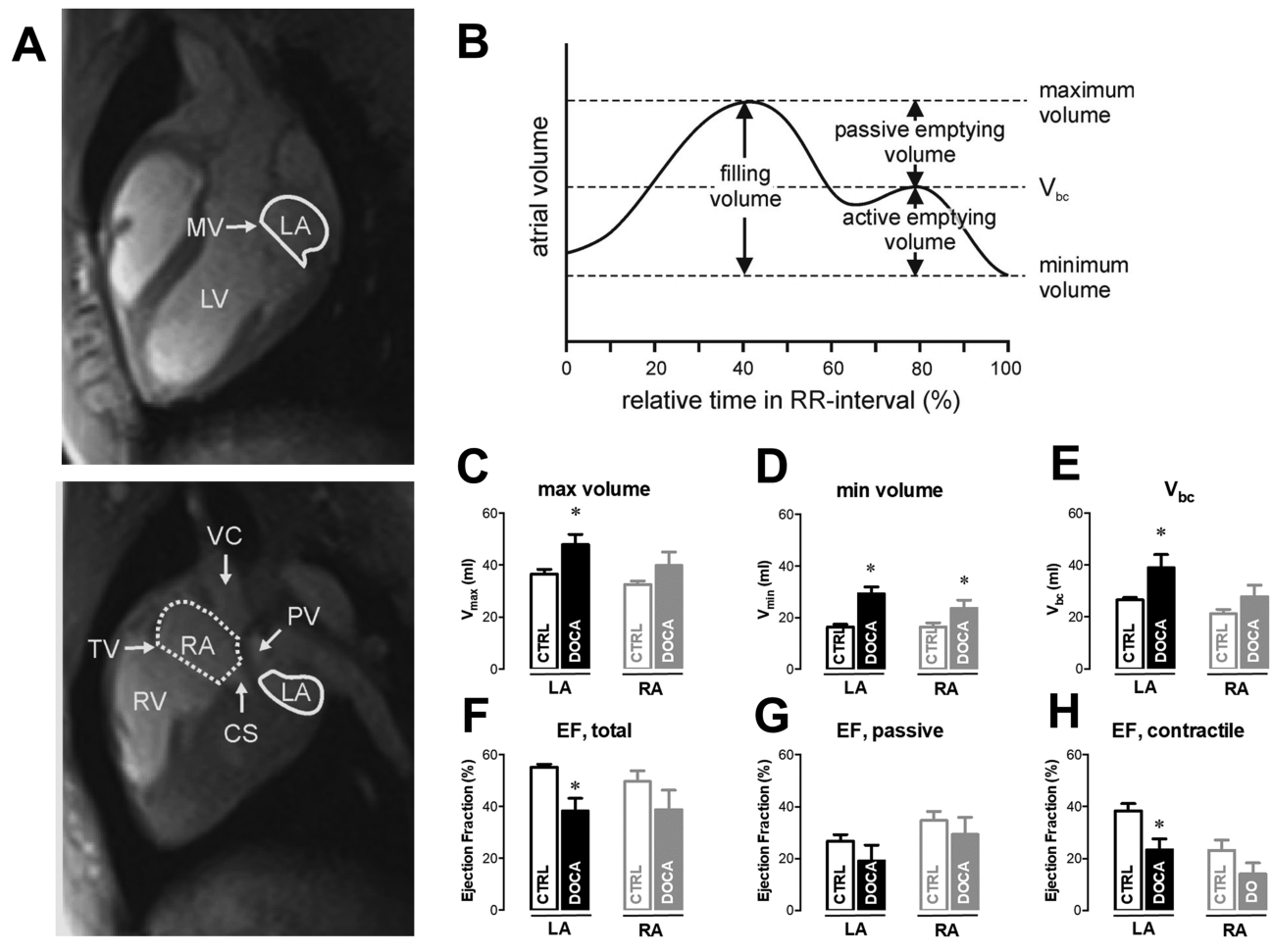
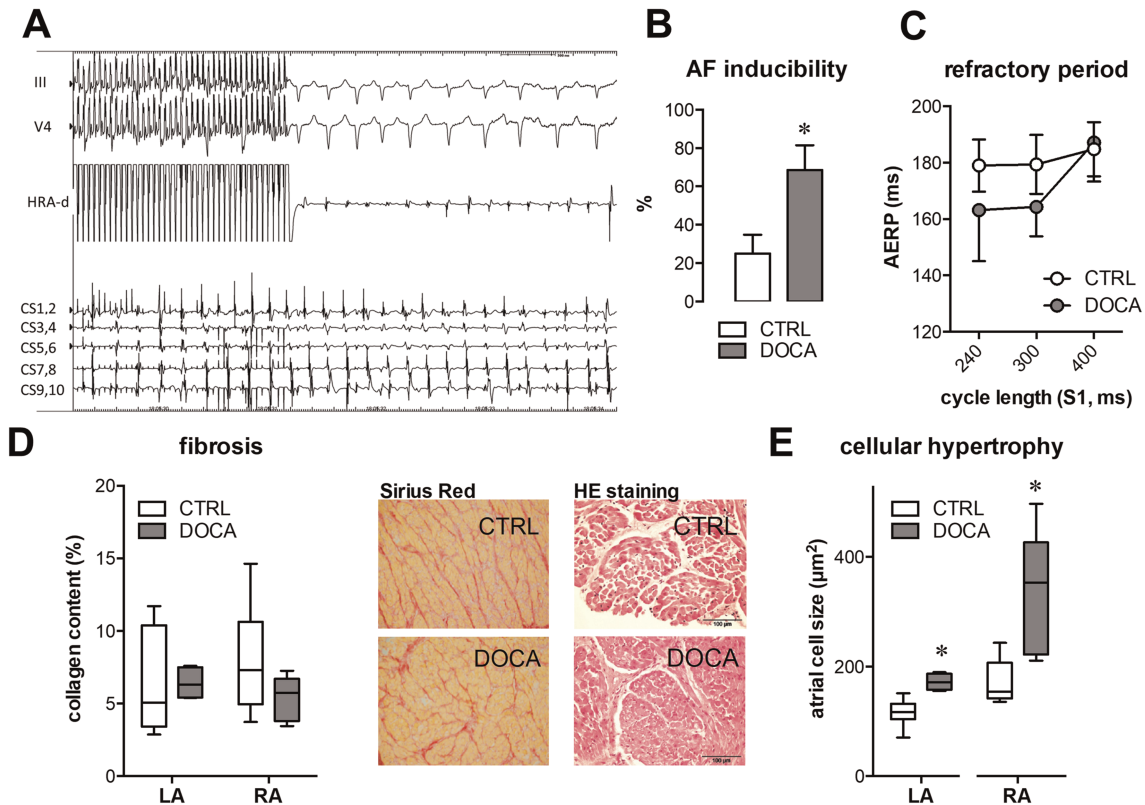


Figure 2 Electrical and histological characteristics of left atrial (LA) and right atrial (RA) remodelling with chronic arterial hypertension. (A) Example of an atrial fibrillation (AF) episode induced by repetitive burst pacing in an 11-deoxycorticosterone acetate (DOCA)-treated pig [50 ms (pacing) cycle length for 10 s]. Traces from top to bottom: two surface electrocardiograms, bipolar electrogram from stimulation site in high right atrium, and five bipolar electrograms from decapolar catheter in coronary sinus. (B) AF inducibility after 50 ms burst pacing is significantly higher in the DOCA group. Data are expressed as mean inducibility during five burst repetitions in each subject. (C) Right atrial effective refractory period (AERP, ms) assessed by a S1–S2 protocol at three different S1 cycle lengths (240/300/400 ms). Average data of eight control (CTRL) and seven DOCA pigs (mean \pm standard error of the mean, n.s.). (D) Representative Sirius Red stainings of atrial tissue from a DOCA and CTRL pig for assessment of collagen content. Pooled data show no difference in LA and RA or between groups. (E) Histological analysis of myocyte area from haematoxylin–eosin (HE) stainings. Samples are from the same animals as in (D) ($N_{CTRL} = 7$; $N_{DOCA} = 8$).



1.2, pyruvate 2, Na L-lactate 1, glucose 12.5, and 2,3-butanedione monoxime 20). LA and RA were alternately assigned to cell isolation and to sampling of tissue for histological and protein expression studies.

For myocyte isolation, intact atria were cannulated through the left circumflex artery (LA cells) or right coronary artery (RA cells) and mounted on a Langendorff set-up. Ventricles were removed, perfusion was checked, and leaky atrial branches were ligated. The atria were perfused using a Ca^{2+} -free Tyrode's solution (in mM: NaCl 130, KCl 5.4, MgSO_4 1.2, pyruvate 2, Na L-lactate 1, and glucose 12.5) for 10 min. Liberase (in mg/mL: CTRL 0.12 and DOCA 0.18, Roche, USA) was added, and perfusion continued for 25 min. After washout of the enzyme solution, tissue was cut into small pieces for mechanical dispersion, followed by stepwise increase of $[\text{Ca}^{2+}]$ in the external solution to 1.8 mM. Myocytes were stored at room temperature and used for experiments within 8 h.

Cardiomyocyte Ca and contractility

Changes in intracellular Ca and cell length were recorded simultaneously in Fura-2AM-loaded cells (1 μM) during field stimulation (0.5–2 Hz). Cell shortening was monitored with a video-based sarcomere length detection system (Myocam and SarLen, IonOptix Corporation) at 120 Hz frame rate and expressed as fractional shortening, that is, normalized to resting sarcomere length, $\Delta L/L_0$. Changes in Ca were expressed as Fura-2 emission ratio (F_{340}/F_{380} , Myocyte Calcium and Contractility System, IonOptix, on a Zeiss Axiovert 200 Microscope). For caffeine experiments, the cells were plated on laminin-coated glass coverslips to avoid moving artefacts of the cell during fast solution switches. The sarcoplasmic reticulum (SR) Ca content was qualitatively assessed by the amplitude of the caffeine-induced Ca transient (20 mM) following 1 Hz stimulation. As an indirect indication of release efficiency, we estimated fractional release by normalizing the

amplitude of the stimulated Ca^{2+} transient (CaT) to SR Ca load ($\Delta\text{CaT}/\text{caffT}$). Ca decline in the presence of caffeine was fitted by a single exponential and is expressed as the decay time constant, τ_{caff} . In the presence of caffeine, this parameter mainly reflects Ca removal by NCX. The decay constant of the CaT during steady-state electrical stimulation attributed to SR Ca^{2+} -ATPase (SERCA) activity (τ_{SERCA}) was calculated from the decay constant of the Ca transient (τ_{SS}) and τ_{caff} obtained from the same cell as previously described.¹⁴

Caffeine was applied before and after 8 min wash-in of 3 μM ORM-10103 to inhibit NCX.¹⁵ The drug (Orion Pharma, Espoo, Finland) was kindly provided by Dr Acsai. Experiments were performed at 37°C.

Histology and immunoblotting

For histological analysis of fibrosis, atrial tissue samples were collected and embedded in formalin and stained with Picrosirius Red to assess collagen content. Cell size was quantified as cross-sectional myocyte area in haematoxylin–eosin-stained tissue slices. Myocyte area of at least 50 cardiomyocytes per animal and region (LA/RA) were measured at $\times 200$ total magnification in 5 μm slices in a central plane, that is, at the level of the nucleus. Image analysis (outlining and area calculation) was performed with ImageJ (Version 1.47, National Institutes of Health). For Western blot analysis, tissue samples were snap frozen in liquid nitrogen and stored at -80°C till homogenization. Separation by sodium dodecyl sulfate–polyacrylamide gel electrophoresis and Western blot was performed according to standard immunoblotting procedures. Membranes were probed with anti-SERCA2a (1/3000, Badrilla, UK), anti-NCX (1/5000, Abnova), anti-phospho-Ser16 phospholamban (PLB) (1/17 000, Badrilla), anti-phospho-Thr17 PLB (1/25 000, Badrilla), anti-PLB (1/5000, Abcam), anti-plasmalemmal Ca pump (1/1000, Santa Cruz, USA), anti-calsequestrin (1/5000, Thermo Scientific, Germany), and anti-glyceraldehyde 3-phosphate dehydrogenase (Abcam, UK). Anti-rabbit or anti-mouse immunoglobulin G linked with horseradish peroxidase (GE Healthcare) were used as a secondary antibody. Ponceau S staining was used to normalize protein expression. Data were averaged from three replicate gels for each sample.

Statistical analysis

Average data are presented as mean \pm standard error of the mean. N refers to number of animals, and n refers to number of cells. For comparisons between groups, unpaired Student's t -test or one-way ANOVA was used. Drug effects within groups were analysed using Student's t -test for paired measurements. For frequency-dependent effects, two-way

ANOVA for repeated measurements was used with Bonferroni *post hoc* testing. Data analysis was performed in GraphPad Prism 6. Differences were considered significant when $P < 0.05$.

Results

After 12 weeks of DOCA plus high-salt/glucose diet, non-invasive systolic blood pressure was significantly higher as compared with CTRL (142 ± 37 mmHg in DOCA vs. 97 ± 6 mmHg in CTRL, $P < 0.001$, Table 1). DOCA pigs developed signs of LV hypertrophy evidenced by an increase in LV mass (134 ± 9 vs. 100 ± 7 g, $P < 0.05$). Magnetic resonance imaging (MRI) studies in a subgroup of animals revealed that LV end-diastolic volume and LV end-systolic volume remained unchanged and that LVEF was preserved ($53 \pm 2\%$ in DOCA vs. $52 \pm 1\%$ in CTRL, n.s., Table 1). All pigs were in sinus rhythm (86 ± 4 b.p.m. in DOCA vs. 89 ± 2 b.p.m. in CTRL under anaesthesia).

Atrial contractility is impaired in hypertensive pigs

In vivo LA and RA function were studied by MRI (Figure 1). LA end-diastolic (LA V_{max}), end-systolic volumes (LA V_{min}), and LA volumes before contraction (LA V_{bc}) were larger in DOCA pigs (LA V_{max} 48 ± 4 vs. 37 ± 2 mL, LA V_{min} 29 ± 3 vs. 16 ± 1 mL, and LA V_{bc} 39 ± 5 vs. 27 ± 1 mL; DOCA vs. CTRL, all $P < 0.05$, Figure 1C–1E). This was associated with an impaired total LAEF largely due to a reduced contractile EF in the DOCA group (LAEF $38 \pm 5\%$ vs. $55 \pm 1\%$, LA contractile EF $23 \pm 4\%$ vs. $38 \pm 3\%$; DOCA vs. CTRL, $P < 0.05$, Figure 1F–1H). In RA, maximum volume and EF (total, contractile, and passive) were not significantly reduced indicating a compensatory state (Figure 1D), but there was a trend towards

Table 1 BP and LV function in the DOCA model

	CTRL ($n = 7$)	DOCA ($n = 5$)	P
BP (mmHg)	97 ± 6	142 ± 37	0.0003
HR (b.p.m.)	89 ± 2	86 ± 4	0.42
LVESV (mL)	43 ± 1	45 ± 5	0.98
LVEDV (mL)	111 ± 3	108 ± 8	0.86
LVEF (%)	52 ± 1	53 ± 2	0.99
LV mass (g)	100 ± 7	134 ± 9	0.014
Weight (kg)	58 ± 3	66 ± 1	0.09

BP, blood pressure; CTRL, control; DOCA, 11-deoxycorticosterone acetate; HR, heart rate; LV, left ventricular; LVEDV, left ventricular end-diastolic volume; LVEF, left ventricular ejection fraction; LVESV, left ventricular end-systolic volume.

The main characteristics of DOCA animals included into the magnetic resonance imaging series. Systolic BP and LV myocardial mass were significantly higher in DOCA animals.

similar changes in total and contractile EF as in LA (Figure 1F–1H, $P = 0.13$ and 0.14 , respectively).

Along with reduced atrial contractile function, DOCA pigs showed a higher inducibility of AF episodes after burst pacing (Figure 2A–2C). Atrial refractory period was not significantly different, although there was a tendency towards shortening in DOCA vs. CTRL at faster pacing cycle lengths (Figure 2C, $P = 0.09$). At tissue level, there were no signs of interstitial fibrosis (Figure 2D). Cardiomyocyte area was larger in LA and RA from DOCA pigs vs. CTRL, indicating cellular hypertrophy in both atria (Figure 2E).

Atrial dysfunction is related to reduced atrial cardiomyocyte contractility

We investigated whether loss of contractile function in the atria was related to reduced intrinsic cardiomyocyte contractile function. Isolated cardiomyocytes from LA and RA were paced at different frequencies, and cytosolic CaTs were measured (Figure 3). Atrial myocytes from healthy pigs showed a

positive cell shortening-frequency response, which was related to a frequency-dependent increase in CaT amplitude. In DOCA cells, the amplitude of contraction and CaT was overall reduced and the positive frequency response was attenuated. The frequency-dependent acceleration of CaT decay and relaxation were preserved in DOCA cells, and relaxation kinetics (not shown) were not different between groups. In the LA but not RA, we observed a small but significant overall prolongation of Ca^{2+} decay in DOCA vs. CTRL, which was more pronounced at lower pacing frequencies (Figure 3A₄ and 3B₄).

Mechanisms of cardiomyocyte dysfunction differ in the right and left atria

In a parallel set of experiments, we performed a more detailed analysis of Ca release and removal. Diastolic cytosolic $[\text{Ca}]_i$ was not changed (Figure 4A₁ and 4B₁, left). In LA cardiomyocytes, reduced CaT amplitude was related to significantly reduced SR Ca^{2+} content; fractional release as a

Figure 3 Reduced left atrial and right atrial cardiomyocyte contraction and calcium transient amplitudes in chronic arterial hypertension. (A) Typical example of simultaneously recorded Ca transient (upper traces) and cell shortening (lower traces) in a control (CTRL) vs. 11-deoxycorticosterone acetate (DOCA) myocyte from the left atrium (A₁) and the right atrium (B₁), 1 Hz. Frequency dependence of fractional cell shortening (L/L_0) (A₂, B₂), Ca transient amplitude (A₃, B₃), and Ca decay (A₄, B₄) in CTRL vs. DOCA cells. Pooled data from the left atrium (CTRL, $n = 12$, $N = 3$, vs. DOCA, $n = 15$, $N = 2$) and the right atrium (CTRL, $n = 13$, $N = 4$, vs. DOCA, $n = 15$, $N = 4$). In both atria, amplitude of contraction and CaT was reduced in DOCA compared with CTRL (# indicates $P < 0.05$ vs. CTRL; * $P < 0.05$, ** $P < 0.01$, and *** $P < 0.001$ vs. 1 Hz).

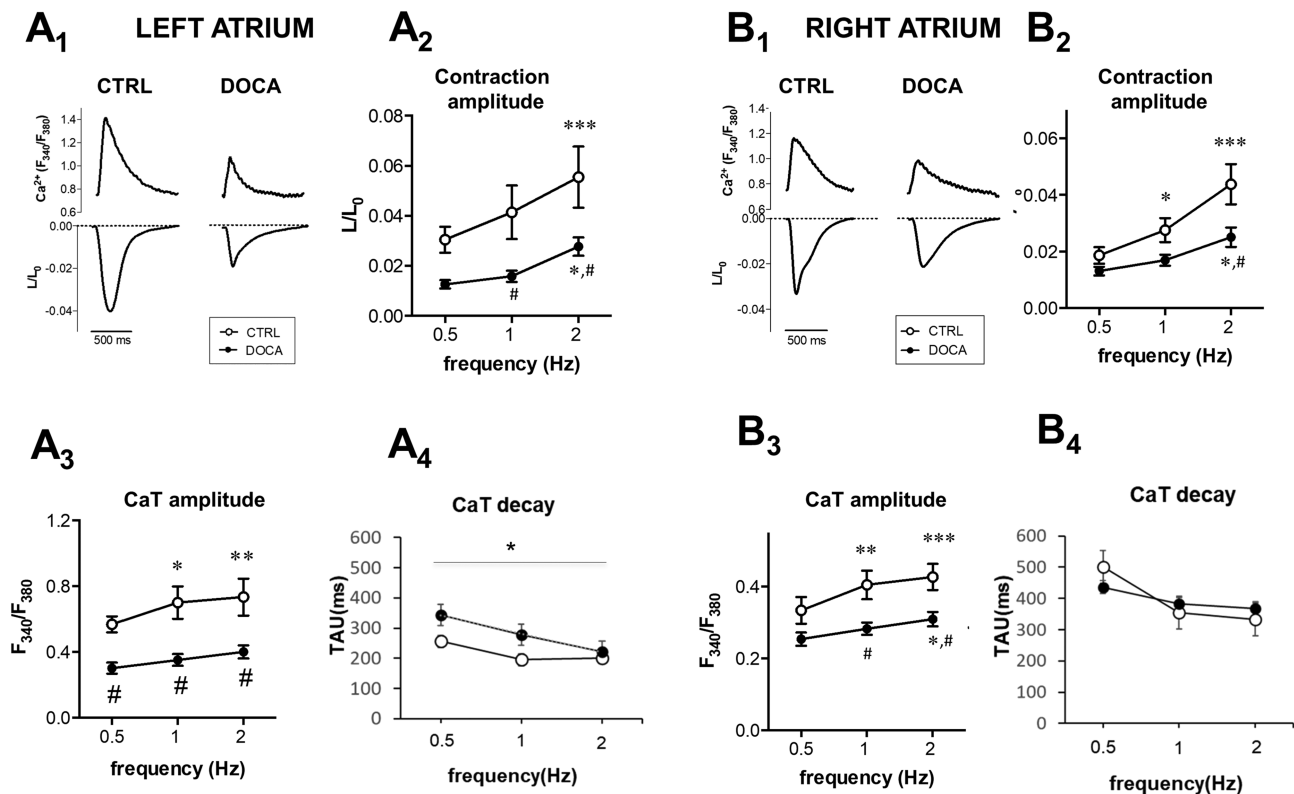
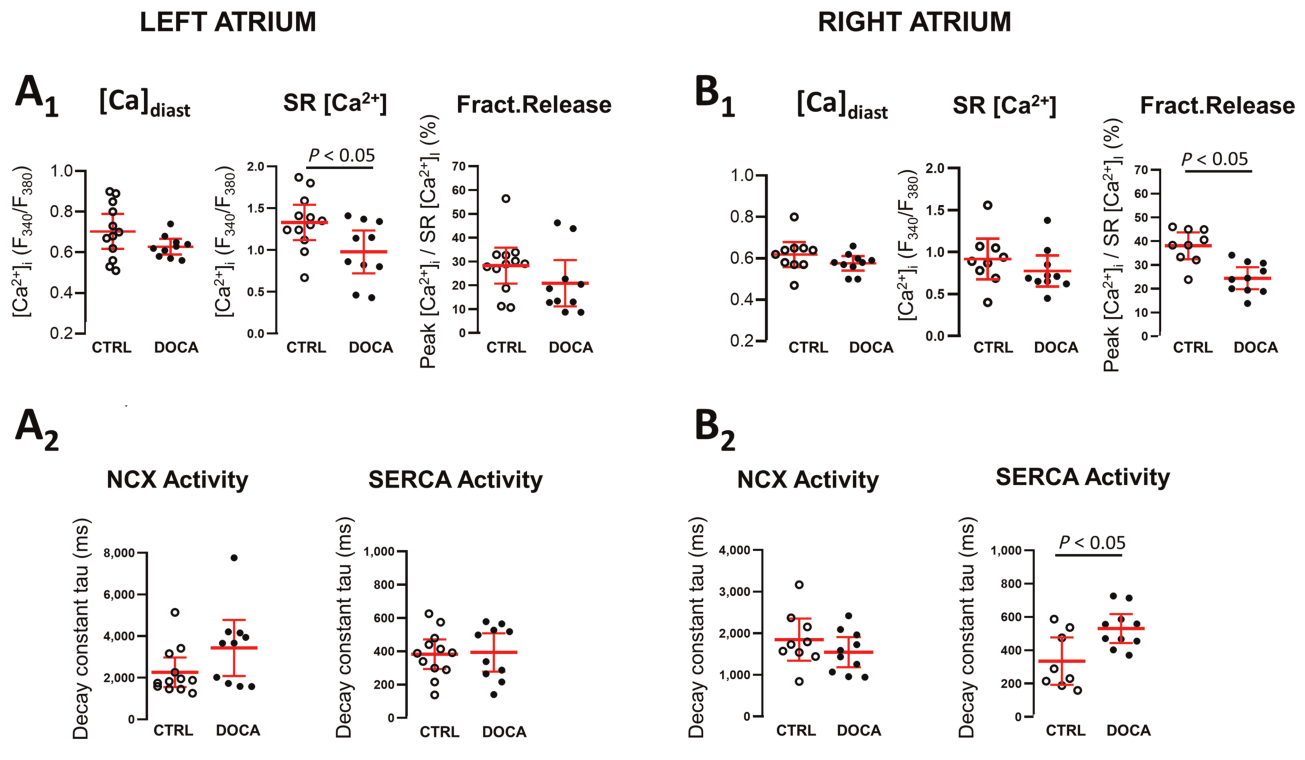


Figure 4 Regulation of Ca release and removal is different between the left and right atria in hypertension. Detailed analysis of steady-state diastolic (A_1 and B_1 , left), sarcoplasmic reticulum $[Ca^{2+}]_i$ (amplitude of caffeine-induced CaT; A_1 and B_1 , middle), and fractional release (FR, A_1 and B_1 , right) in 11-deoxycorticosterone acetate (DOCA) and control (CTRL) left and right atrial cardiomyocytes (left atrium: $N_{CTRL} = 5$, $n = 17$; $N_{DOCA} = 3$, $n = 12$; right atrium: $N_{CTRL} = 5$, $n = 14$; $N_{DOCA} = 3$, $n = 10$). Decline of steady-state Ca transients (τ_{SS}) was fitted by single exponential. Ca removal by sodium–calcium exchanger (NCX) was derived from the decay constant of CaT_{caff} (τ_{caff} , A_2 and B_2 , left). Sarcoplasmic reticulum Ca^{2+} -ATPase (SERCA) activity was calculated from τ_{caff} and τ_{SS} (see Methods for details).



measure of the efficacy of Ca^{2+} -induced Ca^{2+} release was not significantly changed (Figure 4A₁). In RA, reduced CaT amplitude was related to reduced Ca^{2+} -induced Ca^{2+} release efficacy, whereas SR Ca^{2+} content was not significantly changed (Figure 4B₁).

The decline of the Ca transient during a caffeine response is mainly mediated by NCX, and thus, the decay constant (τ_{caff}) is a measure of NCX forward mode activity (i.e. Ca extrusion in exchange for Na influx). In DOCA, NCX forward mode activity was not significantly altered (Figure 4A₂ and 4B₂). Similarly, at the protein expression level, we did not detect differences in the abundance of NCX, SERCA, the plasmalemmal Ca pump, or PLB phosphorylation (Supporting Information, Figure S2).

Partial sodium–calcium exchanger inhibition improves atrial contractility of the left atrium, but not in the right atrium

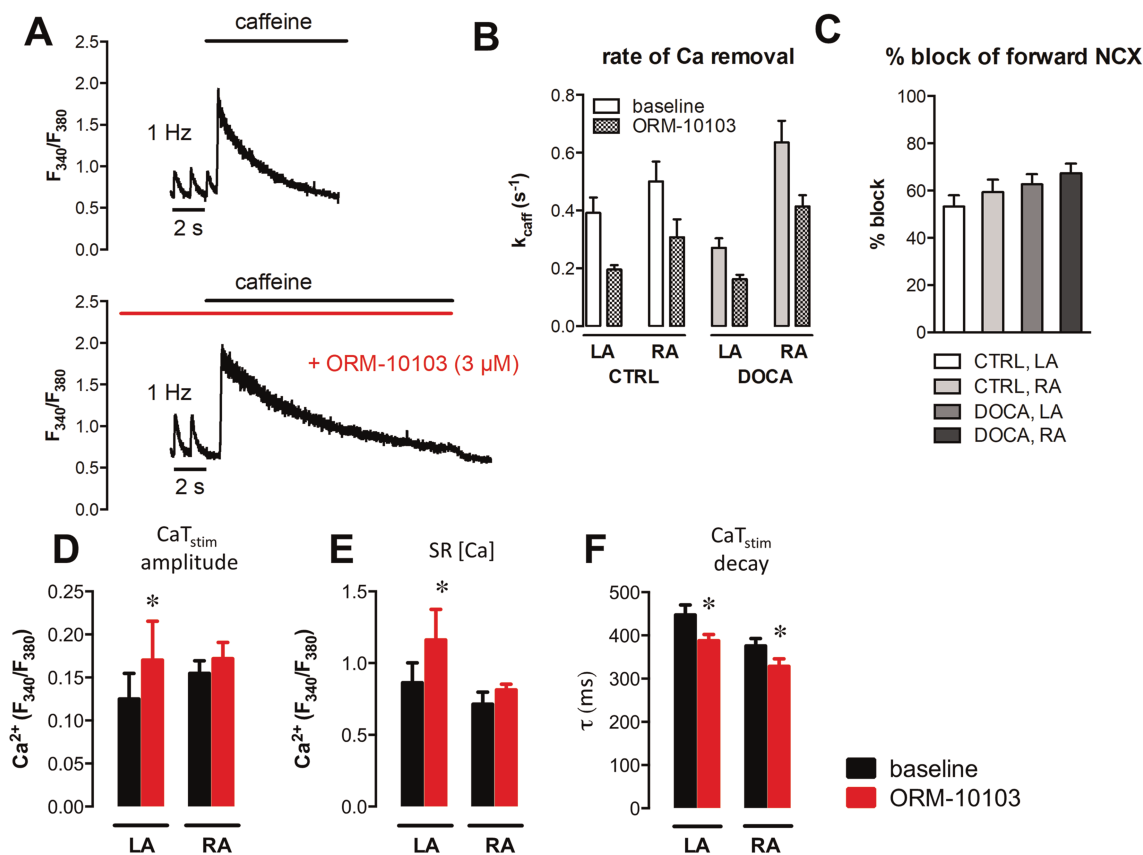
In a subset of cells, we examined if partial NCX block had a positive inotropic effect on atrial contraction by increasing cellular Ca load through inhibition of forward mode NCX, thus

preventing Ca removal from the cell. ORM-10103 slowed the rate of Ca decline (Figure 5A), confirming effective inhibition of NCX. Inhibition was comparable between LA and RA, CTRL and DOCA (Figure 5B), blocking 50–70% of NCX activity (Figure 5C). Indeed, inhibition of NCX induced an increase in CaT amplitude and SR Ca content in LA, but not in RA (Figure 5D and 5E). Interestingly, CaT decay was significantly accelerated by NCX inhibition in LA and RA (Figure 5F).

Discussion

In this study, we have investigated atrial remodelling and atrial function in a large animal model of HHD. We demonstrate that LA remodelling and LA dysfunction occur in the absence of LA fibrosis and show that LA dysfunction was related to contractile dysfunction of the hypertrophied LA cardiomyocytes. Cellular dysfunction was also observed in RA cardiomyocytes. Here, we provide evidence that the mechanisms of maladaptation differ in LA and RA cardiomyocytes and, furthermore, that dysfunctional LA and

Figure 5 Effects of sodium–calcium exchanger (NCX) inhibition with ORM-10103 on Ca transients and sarcoplasmic reticulum (SR) Ca in the left (LA) and right atria (RA). (A) Typical example of a caffeine-induced Ca transient after 1 Hz stimulation at baseline (top) and after wash-in of 3 μ M ORM-10103 (bottom). (B) Rate of Ca removal during caffeine response, k_{caff} (1/s, single exponential fitting), was slower with ORM-10103 in all groups (LA: $N_{\text{CTRL}} = 2, n = 7$; $N_{\text{DOCA}} = 2, n = 8$; RA: $N_{\text{CTRL}} = 2, n = 6$; $N_{\text{DOCA}} = 3, n = 10$). (C) Percentage of forward mode NCX block, calculated from the relative changes in values of caffeine decay constant in (B). (D–F) Detailed analysis of systolic and caffeine-induced Ca transients at baseline and after application of ORM-10103; comparison between 11-deoxycorticosterone acetate (DOCA) LA and RA cardiomyocytes from the same dataset as in *Figure 4*. (D) Systolic Ca transient amplitude at 1 Hz. (E) SR $[\text{Ca}^{2+}]_i$. (F) Time constant of systolic Ca transient decline, τ in ms, obtained from mono-exponential fitting. * $P < 0.05$ vs. baseline; # $P < 0.05$ for comparison between LA and RA. CTRL, control



RA cardiomyocytes respond differently to a targeted therapeutic approach with an NCX inhibitor.

Arterial hypertension is a common trigger of LV remodeling, often resulting in HHD with LV diastolic dysfunction and LA enlargement.⁵ LA enlargement is also a hallmark of HF with preserved EF.¹ Animals in the current model did not show signs or symptoms of HF at baseline (LV end-diastolic pressure and cardiac output at rest were unchanged as previously reported). However, in an earlier study, we could show that the cardiac functional reserve was reduced during dobutamine stress.¹⁶ These findings may be interpreted as early signs of HF with preserved EF¹⁷ and emphasize the role of stress testing as recently recommended.¹⁸

Left atrial dysfunction contributes to reduced exercise tolerance and is prognostically relevant.^{2–4} The mechanisms leading to LA dysfunction and the prevalence of RA dysfunction, however, are not well understood. In patients with (paroxysmal or persistent) AF, LA dysfunction has been

associated with atrial fibrosis.¹⁹ Yet little is known about the prevalence of atrial fibrosis in patients with atrial dysfunction in the absence of AF. Interestingly, in the present model of HHD, LA and RA dysfunction occurred in the absence of atrial fibrosis, while in other animal models of arterial hypertension, atrial fibrosis was detected.^{20–22} In contrast to these models of aortic banding and renovascular hypertension, the present DOCA model mimics low-renin hypertension, which is observed in about one-third of all patients with arterial hypertension.²³ Our observations are in line with a strong role of renin–angiotensin system activation as a trigger for atrial fibrosis.⁷ In a previous study, however, we demonstrated that DOCA-induced arterial hypertension does promote atrial fibrosis in the presence of atrial tachycardia.⁹ Thus, combining our results provides evidence that common risk factors such as arterial hypertension and atrial tachyarrhythmia—while similarly promoting an arrhythmogenic substrate (see *Figure 2* and Manning *et al.*⁹)—lead

to aetiology-specific structural atrial remodelling. We cannot exclude that atrial fibrosis may contribute to atrial dysfunction in our model at later disease stages. For instance, atrial fibrosis was observed (only) with long-standing arterial hypertension in spontaneously hypertensive rats.¹⁰ In line with such late changes, low-voltage areas in atrial myocardium suggestive of increased fibrosis were found in patients with long-standing arterial hypertension.²⁴

While atrial myocyte function has been extensively studied in the context of atrial remodelling driven by AF, only a few studies investigated atrial myocyte function in rodent models of HHD.^{10,12,13} In ageing spontaneously hypertensive rats, alterations in Ca homeostasis occurred early in LA cardiomyocytes, even before cardiomyocyte hypertrophy but with the onset of atrial fibrosis.¹³ However, despite reduced Ca influx through L-type Ca channels and reduced RyR expression, the amplitude and kinetics of LA cardiomyocyte CaT remained compensated. Only at later stages, in the transition from ageing HHD to HF with reduced EF and overt LA enlargement, CaT amplitudes, SR Ca content, and SERCA function in LA myocytes were reduced.¹² Reduced LA cardiomyocyte CaT amplitudes with reduced SR Ca content were also reported after aortic banding in rats.²⁵ In contrast, we have shown in another model of HHD with increased LVEDP (ZSF-1 lean rats) and a preserved LAEF that the CaT amplitude in LA cardiomyocytes was increased vs. wild type, suggesting compensation of increased LA mechanical load.²⁶ In HHD combined with metabolic syndrome, however, LA function *in vivo* deteriorated despite increased LA cardiomyocyte CaT amplitude, possibly related to increased atrial fibrosis.²⁶

The present study sheds light on cellular mechanisms of atrial dysfunction in a large animal model with heart size comparable with human. At the stage of manifest atrial remodelling *in vivo*, LA cardiomyocytes failed to compensate increased mechanical load but rather contributed to deterioration of LA function by a reduced contractility at baseline and reduced contractile reserve. Reduced CaT amplitude despite unchanged SERCA expression suggests a reduced availability of Ca to trigger Ca-induced Ca release. Similar changes have been observed in senescent human atrial cardiomyocytes,²⁷ suggesting that age and mechanical load may synergistically contribute to atrial myocyte dysfunction.

Interestingly, in the present large animal model of HHD, RA cardiomyocyte contractile function was also significantly impaired. As outlined earlier and reviewed earlier,¹ mechanical load is an important trigger for atrial remodelling. Increased RA volume in DOCA *in vivo* suggests that mechanical stress also served as a trigger for RA remodelling. Systemic neurohumoral overactivation is an additional external trigger that may have affected both RA and LA remodelling. Indeed, while DOCA treatment suppresses renin-angiotensin system activity (reduced plasma renin activity, levels of angiotensin I and II, and aldosterone), sympathetic activation as reflected

by plasma norepinephrine is elevated in DOCA pigs even at low DOCA.²⁸ Thus, while RA and LA have experienced similar triggers of remodelling, preserved SR Ca and increased NCX activity in RA vs. LA cardiomyocytes suggests that RA and LA cardiomyocytes responded differentially to these external stressors. These differences may in part be related to the extent and relation of mechanical, neurohumoral and possibly paracrine stress sensed by the RA vs. the LA. In addition, an intrinsic diversity in the stress response between RA and LA cardiomyocytes was recently suggested, which may contribute to our observed differences between LA and RA and warrants further study.²⁹

The sarcolemmal NCX exports Ca out of the cytosol in exchange for Na (forward mode) generating a potentially arrhythmogenic depolarizing inward current. NCX inhibitors have shown to reduce arrhythmias and also have the potential to increase cardiomyocyte inotropy by augmenting cytosolic Ca.³⁰ We used the NCX inhibitor ORM-10103, a new compound with improved NCX specificity and no effects on L-type Ca influx.³¹ Partial NCX inhibition might be an interesting strategy to improve atrial contractility in salt-sensitive hypertension because of its documented blood pressure lowering effects in this condition.¹⁴ Indeed, we found that ORM-10103 increases CaT amplitude and SR Ca in LA cardiomyocytes from DOCA (*Figure 5D*). This was not associated with a slowed but rather an accelerated Ca removal from the cytosol, which may be explained by reduced competition for SERCA-mediated Ca removal or the inhibition of additional reverse mode activity of the NCX at different phases of the cardiac cycle as described earlier.³² The response of RA cardiomyocytes to NCX inhibition (*Figure 5D–5F*) suggested that in RA vs. LA cardiomyocytes, NCX activity may be shifted more to reverse mode (Ca import) during the cardiac cycle.

Limitations

In the present model, non-invasive blood pressure was measured only at the end of the observation period to minimize the number of anaesthesia per animal (3R). However, DOCA sustained release pellets are a well-established intervention to induce elevated blood pressure, and we have previously reported a robust and reproducible increase in arterial blood pressure in this model.^{16,17,33} DOCA pigs tended to have a higher body weight than CTRL at the time of final experiment (*Table 1*). However, similar systolic and diastolic LV volumes in both groups suggest that the observed trend in body weight had little impact on cardiac cavity size. Our measurements in isolated cardiomyocytes point at impaired Ca homeostasis with intrinsic atrial myocyte dysfunction as the cellular substrate for atrial cardiomyopathy in this model; however, upstream intracellular and potential extracellular signalling needs to be further

explored. While we have investigated the potential benefit of NCX inhibition to increase SR Ca and improve CaT amplitudes in diseased animals as a proof of concept, we did not extend this approach to healthy animals. We believe our results provide proof of concept for an effect in diseased animals and evidence for a subsequential in-depth pharmacodynamic safety evaluation of NCX inhibition on atrial function *in vitro* and *in vivo*.

In summary, in this large animal model of HHD, atrial remodelling and contractile dysfunction occur in the absence of atrial fibrosis. Cardiomyocyte contractile dysfunction with reduced inotropy is present in LA and also in RA in the absence of HF. Improving atrial cardiomyocyte inotropy should be evaluated as a therapeutic aim in HHD.

Conflict of interest

None declared.

References

- Hohendanner F, Messroghli D, Bode D, Blaschke F, Parwani A, Boldt LH, Heinzel FR. Atrial remodelling in heart failure: recent developments and relevance for heart failure with preserved ejection fraction. *ESC Heart Fail* 2018; **5**: 211–221.
- Santos AB, Roca GQ, Claggett B, Sweitzer NK, Shah SJ, Anand IS, Fang JC, Zile MR, Pitt B, Solomon SD, Shah AM. Prognostic relevance of left atrial dysfunction in heart failure with preserved ejection fraction. *Circ Heart Fail* 2016; **9**: e002763.
- von Roeder M, Rommel KP, Kowallick JT, Blazek S, Besler C, Fengler K, Lotz J, Hasenfuß G, Lücke C, Gutberlet M, Schuler G. Influence of left atrial function on exercise capacity and left ventricular function in patients with heart failure and preserved ejection fraction. *Circ Cardiovasc Imaging* 2017; **10**: e005467.
- D'Andrea A, Caso P, Romano S, Scarafite R, Cuomo S, Salerno G, Riegler L, Limongelli G, Di Salvo G, Romano M, Luccardo B. Association between left atrial myocardial function and exercise capacity in patients with either idiopathic or ischemic dilated cardiomyopathy: a two-dimensional speckle strain study. *Int J Cardiol* 2009; **132**: 354–363.
- Cuspidi C, Rescaldani M, Sala C. Prevalence of echocardiographic left-atrial enlargement in hypertension: a systematic review of recent clinical studies. *Am J Hypertens* 2013; **26**: 456–464.
- Tadic M, Cuspidi C, Suzic-Lazic J, Andric A, Stojceviski B, Ivanovic B, Hot S, Scepanovic R, Celic V. Is there a relationship between right-ventricular and right atrial mechanics and functional capacity in hypertensive patients? *J Hypertens* 2014; **32**: 929–937.
- Goette A, Kalman JM, Aguinaga L, Akar J, Cabrera JA, Chen SA, Chugh SS, Corradi D, D'Avila A, Dobrev D, Fenelon G. EHRA/HRS/APHS/SOLAECE expert consensus on atrial cardiomyopathies: definition, characterization, and clinical implication. *Europace* 2016; **18**: 1455–1490.
- Wijffels MC, Kirchhof CJ, Dorland R, Allesie MA. Atrial fibrillation begets atrial fibrillation: a study in awake chronically instrumented goats. *Circulation* 1995; **92**: 1954–1968.
- Manninger M, Zweiker D, van Hunnik A, Alogna A, Prassl AJ, Schipke J, Zeemering S, Zirngast B, Schönleitner P, Schwarzl M, Herbst V. Arterial hypertension drives arrhythmia progression via specific structural remodeling in a porcine model of atrial fibrillation. *Heart Rhythm* 2018; **15**: 1328–1336.
- Lau DH, Shipp NJ, Kelly DJ, Thanigaimani S, Neo M, Kuklik P, Lim HS, Zhang Y, Drury K, Wong CX, Chia NH. Atrial arrhythmia in ageing spontaneously hypertensive rats: unraveling the substrate in hypertension and ageing. *PLoS ONE* 2013; **8**: e72416.
- Lau DH, Mackenzie L, Kelly DJ, Psaltis PJ, Brooks AG, Worthington M, Rajendram A, Kelly DR, Zhang Y, Kuklik P, Nelson AJ. Hypertension and atrial fibrillation: evidence of progressive atrial remodeling with electrostructural correlate in a conscious chronically instrumented ovine model. *Heart Rhythm* 2010; **7**: 1282–1290.
- Pluteanu F, Nikonova Y, Holzapfel A, Herzog B, Scherer A, Preisenberger J, Plačkić J, Scheer K, Ivanova T, Bukowska A, Goette A. Progressive impairment of atrial myocyte function during left ventricular hypertrophy and heart failure. *J Mol Cell Cardiol* 2018; **114**: 253–263.
- Pluteanu F, Hess J, Plackic J, Nikonova Y, Preisenberger J, Bukowska A, Schotten U, Rinne A, Kienitz MC, Schäfer MK, Weihe E. Early subcellular Ca²⁺ remodeling and increased propensity for Ca²⁺ alternans in left atrial myocytes from hypertensive rats. *Cardiovasc Res* 2015; **106**: 87–97.
- Iwamoto T, Kita S, Zhang J, Blaustein MP, Arai Y, Yoshida S, Wakimoto K, Komuro I, Katsuragi T. Salt-sensitive hypertension is triggered by Ca²⁺ entry via Na⁺/Ca²⁺ exchanger type-1 in vascular

Funding

This work was supported by the European Commission (Grant No. 261057; European Network for Translational Research in Atrial Fibrillation (EUTRAF), Grant No. 633196. M.M. and G.J. received funding from the Medical University of Graz (Medizinische Universität Graz) within the PhD Program Molecular Medicine. G.J. was supported by the funds of Wenzhou Municipal Science and Technology Bureau (Grant No. Y20160029).

Supporting information

Additional supporting information may be found online in the Supporting Information section at the end of the article.

Figure S1. Animal usage.

Figure S2. Protein expression of NCX, SERCA and PMCA, phosphorylation of phospholamban as determined by Western blot. See text for details.

- smooth muscle. *Nat Med* 2004; **10**: 1193–1199.
15. Nagy N, Kormos A, Kohajda Z, Szebeni A, Szepesi J, Pollesello P, Levijoki J, Acsai K, Virág L, Nánási PP, Papp JG. Selective $\text{Na}^+/\text{Ca}^{2+}$ exchanger inhibition prevents Ca^{2+} overload-induced triggered arrhythmias. *Br J Pharmacol* 2014; **171**: 5665–5681.
 16. Schwarzl M, Hamdani N, Seiler S, Alogna A, Manninger M, Reilly S, Zirngast B, Kirsch A, Steendijk P, Verderber J, Zweiker D. A porcine model of hypertensive cardiomyopathy: implications for heart failure with preserved ejection fraction. *Am J Physiol Heart Circ Physiol* 2015; **309**: H1407–H1418.
 17. Reiter U, Reiter G, Manninger M, Adelsmayr G, Schipke J, Alogna A, Rajces A, Stalder AF, Greiser A, Mühlfeld C, Scherr D. Early-stage heart failure with preserved ejection fraction in the pig: a cardiovascular magnetic resonance study. *J Cardiovasc Magn Reson* 2016; **18**: 63.
 18. Pieske B, Tschöpe C, de Boer RA, Fraser AG, Anker SD, Donal E, Edelmann F, Fu M, Guazzi M, Lam CS, Lancellotti P. How to diagnose heart failure with preserved ejection fraction: the HFA-PEFF diagnostic algorithm: a consensus recommendation from the Heart Failure Association (HFA) of the European Society of Cardiology (ESC). *Eur J Heart Fail* 2020; **22**: 391–412.
 19. Habibi M, Lima JA, Khurram IM, Zimmerman SL, Zipunnikov V, Fukumoto K, Spragg D, Ashikaga H, Rickard J, Marine JE, Calkins H. Association of left atrial function and left atrial enhancement in patients with atrial fibrillation: cardiac magnetic resonance study. *Circ Cardiovasc Imaging* 2015; **8**: e002769.
 20. Lau DH, Mackenzie L, Rajendram A, Psaltis PJ, Kelly DR, Spyropoulos P, Zhang Y, Olakkengil SA, Russell CH, Brooks AG, Faull RJ. Characterization of cardiac remodeling in a large animal “one-kidney, one-clip” hypertensive model. *Blood Press* 2010; **19**: 119–125.
 21. Wei W, Rao F, Liu F, Xue Y, Deng C, Wang Z, Zhu J, Yang H, Li X, Zhang M, Fu Y. Involvement of Smad3 pathway in atrial fibrosis induced by elevated hydrostatic pressure. *J Cell Physiol* 2018; **233**: 4981–4989.
 22. Kim SJ, Choisy SC, Barman P, Zhang H, Hancox JC, Jones SA, James AF. Atrial remodeling and the substrate for atrial fibrillation in rat hearts with elevated afterload. *Circ Arrhythm Electrophysiol* 2011; **4**: 761–769.
 23. Monticone S, Burrello J, Tizzani D, Bertello C, Viola A, Buffolo F, Gabetti L, Mengozzi G, Williams TA, Rabbia F, Veglio F. Prevalence and clinical manifestations of primary aldosteronism encountered in primary care practice. *J Am Coll Cardiol* 2017; **69**: 1811–1820.
 24. Medi C, Kalman JM, Spence SJ, Teh AW, Lee G, Bader I, Kaye DM, Kistler PM. Atrial electrical and structural changes associated with longstanding hypertension in humans: implications for the substrate for atrial fibrillation. *J Cardiovasc Electrophysiol* 2011; **22**: 1317–1324.
 25. Zhang H, Cannell MB, Kim SJ, Watson JJ, Norman R, Calaghan SC, Orchard CH, James AF. Cellular hypertrophy and increased susceptibility to spontaneous calcium-release of rat left atrial myocytes due to elevated afterload. *PLoS ONE* 2015; **10**: e0144309.
 26. Hohendanner F, Bode D, Primessnig U, Guthof T, Doerr R, Jeuthe S, Reimers S, Zhang K, Bach D, Wakula P, Pieske BM. Cellular mechanisms of metabolic syndrome-related atrial decompensation in a rat model of HFpEF. *J Mol Cell Cardiol* 2018; **115**: 10–19.
 27. Herraiz-Martinez A, Alvarez-Garcia J, Llach A, Molina CE, Fernandes J, Ferrero-Gregori A, Rodríguez C, Vallmitjana A, Benítez R, Padro JM, Martínez-González J. Ageing is associated with deterioration of calcium homeostasis in isolated human right atrial myocytes. *Cardiovasc Res* 2015; **106**: 76–86.
 28. Han W, Fang W, Gan Q, Guan S, Li Y, Wang M, Gong K, Qu X. Low-dose sustained-release deoxycorticosterone acetate-induced hypertension in Bama miniature pigs for renal sympathetic nerve denervation. *J Am Soc Hypertens* 2017; **11**: 314–320.
 29. Le QA, Kim JC, Kim KH, Van Vu AT, Woo SH. Distinct shear-induced Ca^{2+} signaling in the left and right atrial myocytes: role of P2 receptor context. *J Mol Cell Cardiol* 2020; **143**: 38–50.
 30. Antoons G, Willems R, Sipido KR. Alternative strategies in arrhythmia therapy: evaluation of Na/Ca exchange as an anti-arrhythmic target. *Pharmacol Ther* 2012; **134**: 26–42.
 31. Jost N, Nagy N, Corici C, Kohajda Z, Horvath A, Acsai K, Biliczki P, Levijoki J, Pollesello P, Koskelainen T, Otsomaa L. ORM-10103, a novel specific inhibitor of the $\text{Na}^+/\text{Ca}^{2+}$ exchanger, decreases early and delayed afterdepolarizations in the canine heart. *Br J Pharmacol* 2013; **170**: 768–778.
 32. Primessnig U, Schonleitner P, Holl A, Pfeiffer S, Bracic T, Rau T, Kapl M, Stojakovic T, Glasnov T, Leineweber K, Wakula P. Novel pathomechanisms of cardiomyocyte dysfunction in a model of heart failure with preserved ejection fraction. *Eur J Heart Fail* 2016; **18**: 987–997.
 33. Alogna A, Schwarzl M, Manninger M, Hamdani N, Zirngast B, Kloth B, Steendijk P, Verderber J, Zweiker D, Westermann D, Blankenberg S. Acute stimulation of the soluble guanylate cyclase does not impact on left ventricular capacitance in normal and hypertrophied porcine hearts in vivo. *Am J Physiol Heart Circ Physiol* 2018; **315**: H669–H680.